Coherent helix vacancy phonon and its ultrafast dynamics waning in topological Dirac semimetal Cd_3As_2

Fei Sun,[1,2] Q. Wu,[1,2] Y. L. Wu,[1] H. Zhao,[1,2] C. J. Yi,[1,2] Y. C. Tian,[1] H. W. Liu,[1] Y. G. Shi,[1]
H. Ding,[1,2,3] X. Dai,[1,2,3] P. Richard,[1,2,3] and Jimin Zhao[1,2,*]

[1]*Beijing National Laboratory for Condensed Matter Physics, Institute of Physics, Chinese Academy of Sciences, Beijing 100190, China*
[2]*School of Physical Sciences, University of Chinese Academy of Sciences, Beijing 100049, China*
[3]*Collaborative Innovation Center of Quantum Matter, Beijing, China*

(Received 5 October 2016; published 5 June 2017; corrected 15 June 2017)

We report an ultrafast lattice dynamics investigation of the topological Dirac semimetal Cd_3As_2. A coherent phonon beating among three evenly spaced A_{1g} optical phonon modes (of frequencies 1.80, 1.96, and 2.11 THz, respectively) is unambiguously observed. The two side modes originate from the counter helixes composing Cd vacancies. Significantly, such helix vacancy-induced phonon (HVP) modes experience prominent extra waning in their ultrafast dynamics as temperature increases, which is immune to the central mode. Above 200 K, the HVP becomes inactive, which may potentially affect the topological properties. Our results in the lattice degree of freedom suggest the indispensable role of temperature in considering topological properties of such quantum materials.

DOI: 10.1103/PhysRevB.95.235108

The theoretical prediction [1,2] and experimental verification [3–5] of the three-dimensional (3D) Dirac semimetals [4] enriched the family of topological quantum materials. It is known that by relieving spatial inversion symmetry, a Dirac semimetal can be transmuted into a Weyl semimetal [2,6], which explicitly gives an example that the crystal lattice may determine the topological property. The x-ray diffraction (XRD) investigations have shown that Cd_3As_2, a typical 3D topological semimetal, preserves a complex crystal structure, where alternating counter helixes of Cd vacancies form a square array [7] at low temperatures. The subtle effect of this lattice structure (including its spatial inversion symmetry) on its topological property has been discussed [7].

However, more detailed knowledge about this lattice structure has not been fully explored. For example, the temperature-dependent lattice collective excitations resulting from the helix of vacancies has not been reported so far, and temperature-dependence evidences of lattice phase transitions, though reported, are not fully explicitly presented [8]. This is mainly because the lattice structure is so complex that a thorough temperature-dependent investigation of the lattice degree of freedom is challenging. Furthermore, since theoretical predictions often refer to 0 K physics and a theoretical prediction of the full lattice phase transition with temperature is challenging, the effect of the lattice (temperature) on topological properties cannot be fully accounted for by theory.

Facing such hidden challenges, we carry out an ultrafast pump-probe optical spectroscopy investigation of a single crystal Cd_3As_2 ranging from 6 to 267 K, assisted by spontaneous Raman scattering. Ultrafast spectroscopy has been employed in observing quantum phase transitions [9–13] and topological properties [14–16]. Owing to its advantages in coherent generation and detection, ultrafast spectroscopy has been also widely used to probe the coherent phonon dynamics in quantum materials [9,17–21]. Other than the helix vacancy-induced phonon modes (abbreviated as HVP), our major discovery is a clear waning (with increasing temperature) behavior in its ultrafast dynamics that is "superimposed" on a regular anharmonic phonon-phonon scattering. Our results suggest the possibility of a more subtle lattice phase transition and that temperature (lattice) may affect the topological properties in similar materials, especially at higher (including room) temperatures.

Our experimental setup is similar to that in Refs. [9,10] and the details are given in the Supplemental Material in Ref. [22]. Ultrafast laser pulses of 800 nm central wavelength, ~70 fs pulse duration, and 250 kHz repetition rate are used, with the pump and probe fluences being 3.42 and 1.33 mJ/cm^2, respectively. Complementary confocal Raman scattering has also been carried out using a 568.2 nm laser beam (see Supplemental Material [22]). The details of our sample preparation was reported in Ref. [23]. We performed x-ray diffraction (XRD) characterization of the single crystal Cd_3As_2 (see Supplemental Material [22]) at room temperature, which shows a tetragonal unit cell with $a = b = 12.67$Å and $c = 25.48$Å and a structure that respects the space group $I4_1/acd$ (no. 142) [7]. Our XRD results also show that the cleaved surface is the (0, 1, 0) plane (see Supplemental Material [22]).

We measure the differential reflectivity $\Delta R/R_0$ of the probe beam as a function of the delay time between the pump and probe beams. This reflects the modification of the dielectric constant by the excited state carriers and lattice collective excitations that are concomitant to the pump beam excitation. By scanning with femtosecond step size, we observe fast oscillation components superimposed on the electronic response right after the pump excitation [Fig. 1(a)]. The inset of Fig. 1(a) illustrates the zoom-in view of these oscillations, which we attribute to coherent optical phonons. We extract and replot these oscillations in Fig. 1(b). Interestingly, a frequency beating can be clearly observed, indicating separate optical phonon modes with slightly different energies. The inset of Fig. 1(b) shows the fast Fourier transformation (FFT) of the time-domain results, explicitly revealing the closely spaced frequency-domain peaks. The three peak values are 1.80, 1.96, and 2.11 THz. We attribute the two side peaks to the slightly

*Corresponding author: jmzhao@iphy.ac.cn

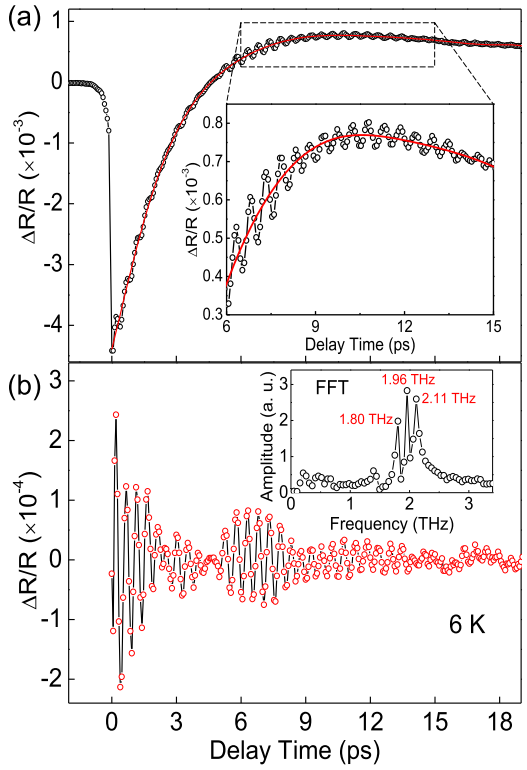

FIG. 1. (a) Ultrafast dynamics at 6 K, with a zoom-in view shown in the inset. The red curve is a fitting to the photocarrier dynamics. (b) Oscillation components obtained by subtracting the fitted curve in (a) from the raw data. Damped oscillations with frequency beating can be clearly identified. The inset is the FFT of the time-resolved oscillation.

different helix vacancy-induced bond strengths [7]. Due to the Cd atom vacancies, some Cd-As bonds are elongated and some others are shortened (Fig. 5), leading to modified vibration frequencies. Since such modified bond lengths have fixed identical values at a given temperature, it is expected that clear peaks with definite frequencies emerge, instead of a continuous broadening of the central peak. This is verified as shown in Fig. 1.

To confirm the above assignment, the coherent phonon beating (CPB) result should be fitted well by adding up three individual coherent optical phonon modes. To do so, we first fit the CPB together with the electronic dynamics by using the following equation:

$$\begin{aligned}\Delta R/R_0 = {} & A_\omega \exp(-t/\tau_\omega)\sin(\omega t+\varphi) + A_{\omega_-}\exp(-t/\tau_{\omega_-}) \\ & \times \sin(\omega_- t+\varphi_-) + A_{\omega_+}\exp(-t/\tau_{\omega_+}) \\ & \times \sin(\omega_+ t+\varphi_+) + A_{\text{fast}}\exp(-t/\tau_{\text{fast}}) \\ & + A_{\text{slow}}\exp(-t/\tau_{\text{slow}}) + A_0, \end{aligned} \quad (1)$$

where ω,ω_-,ω_+ stand for the three frequencies, $A_\omega, A_\omega, A_{\omega+}$ denote amplitudes, $\tau_\omega,\tau_{\omega-},\tau_{\omega+}$ represent phonon lifetimes, and $\varphi,\varphi_-,\varphi_+$ are the corresponding initial phases, respectively. The indexes "fast" and "slow" represent electronic dynamics components, and A_0 is the background mainly from stray pump scattering. Then we subtract the electronic component to get the coherent phonon component, which we simulate by adding up the three optical phonon oscillations (see Supplemental Material [22]). The simulation fits the data well and confirms the assignment of the CPB.

The phases of the phonon oscillations can be observed directly from the time-resolved measurement results. From the fitting, we obtain that the initial phases φ, φ_-, and φ_+ are all 0.09π. Since it is very close to 0, we can attribute the coherent generation of the optical phonons to the impulsive stimulated Raman scattering [24–26]. The point group corresponding to the space group $I4_1/acd$ (no. 142) is D_{4h}, for which the Raman active tensors are listed in the Supplemental Material in Ref. [22]. In the ultrafast spectroscopy that is of impulsive stimulated Raman scattering mechanism, we have $\Delta R/R \propto [\mathbf{e}_{\text{pump}}\cdot\mathbf{R}_0\cdot\mathbf{e}_{\text{probe}}][\mathbf{e}_{\text{probe}}\cdot\mathbf{R}_0\cdot\mathbf{e}_{\text{pump}}]$, where $\mathbf{R}_0$ is the Raman tensor and $\mathbf{e}$ is the light polarization direction. In our experiment, the pump beam is vertically polarized and the probe beam is horizontally polarized. Consequently, the ultrafast spectroscopy geometry allows for the observation of A_{1g} and B_{1g} phonons, which are Raman active (see Supplemental Material [22]).

We further investigate the temperature dependence of the CPB. Figures 2(a) and 2(b) map out the time- and frequency-domain dynamics of the CPB, respectively. With increasing temperature, the two side bands (red dashed lines marked as F_1 and F_3) decay faster than the major central peak at 1.96 THz (red dashed line marked as F_2). Besides, as expected, redshifts of the phonon peaks are easily identified. In contrast, another phonon peak observed at a lower energy (blue dashed line marked as F_0) shows very weak or no redshift.

To further confirm our mode analysis, we performed low-wave-number Raman scattering experiments of Cd_3As_2 at selected temperatures. The results are obtained with the incident polarization parallel to that of the scattered light (XX), as displayed in Fig. 2(c). In this configuration, both modes with the A_{1g} and B_{1g} symmetries are allowed. Unlike for the A_{1g} modes though, the intensity of the peaks with the B_{1g} symmetry should vary significantly with the sample in-plane orientation, which allows us to distinguish between the two symmetries. Five dominant excitations are observed at 46.4, 53.8, 58.6, 64.7, and 68.8 cm^{-1} [Fig. 2(c)]. The right three peaks match well the optical phonon modes at 1.80, 1.96, and 2.11 THz ($F_1 - F_3$) revealed by the ultrafast measurements using a cross-polarization configuration, respectively. The intensity of these Raman excitations is rather insensitive to the sample orientation (see Supplemental Material [22]), indicating A_{1g} modes. The consistency between ultrafast measurements and Raman scattering further allows us to confirm the A_{1g} assignment of these three optical phonons to modes [27,28]. The phonon mode at 46.4 cm^{-1} (1.4 THz) is also detected in the ultrafast measurement, matching peak 1 (F_0) in the Raman scattering spectra. The peak at 53.8 cm^{-1} in Raman scattering is not detected in ultrafast spectroscopy, which might be due to a symmetry that differs from the three optical phonon modes $F_1 - F_3$. Alternatively, this peak may be too weak (compared with the residual of subtracting the electronic dynamics) to detect in our ultrafast experiment (notice the sharp reduction in the amplitude of F_0 as compared with that of peak 1 in the Raman spectra).

Based on the FFT results in Fig. 2(b), we investigate the temperature dependence of the CPB dynamics. The phonon's

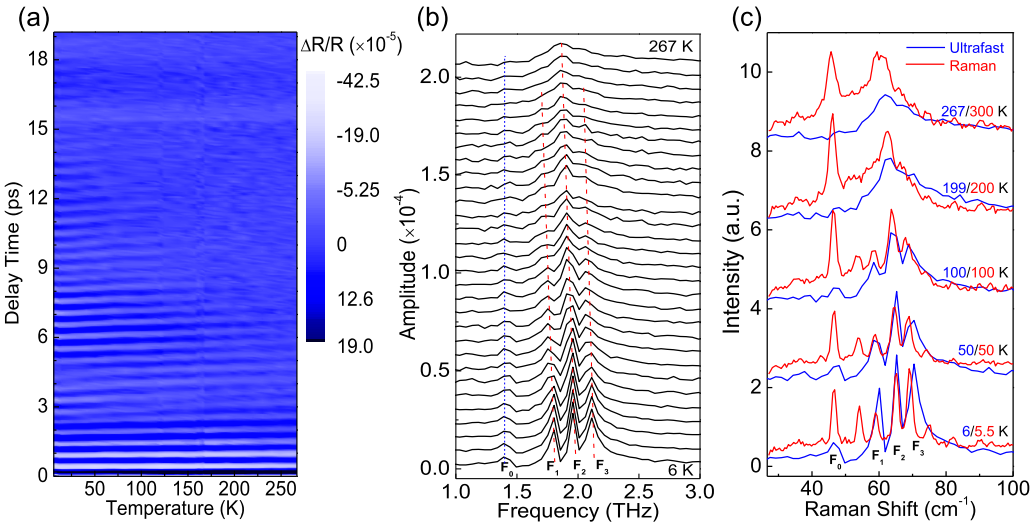

FIG. 2. (a) Color mapping of the optical phonon beating. Other than the apparent oscillation, a frequency beating can also be clearly identified, especially at relatively low temperatures. (b) Phonon peaks (red dashed lines) clearly seen in the corresponding FFT results. The two side peaks damp faster than the major peak with increasing temperature. (c) Comparison with Raman scattering. The two sets of data compare well with each other, including a noticeable redshift with rising temperature. Data are offset in both (b) and (c).

frequency and FFT amplitude are extracted from Fig. 2(b) and plotted in Figs. 3(a) and 3(b), respectively. It is worthwhile to note that the phonon's FFT amplitude is not identical to the phonon amplitude, which we discuss below. The redshifts in F_1,F_2, and F_3 observed in Fig. 2(b) can be clearly identified in Fig. 3(a).

Significantly, the FFT amplitudes of the three phonon oscillations show different attenuation rates with increasing temperature [Fig. 3(b)], which we denote as dynamics waning for the two side modes. These two side HVP modes (F_1 and F_3) exhibit clear waning tendency as compared to the major central peak (F_2). To see this clearly, we use two dashed curves to mark a "regular" temperature-dependence behavior (resulting from regular anharmonic phonon-phonon scattering) and the color bulks to mark the magnitude of the discrepancies [Fig. 3(b)]. Due to the relatively small number of vacancies (two vacancies vs six nonvacancies), it is conceivable that these side optical phonon modes exhibit more sensitive temperature dependences than the central peak. Moreover, the central peak also exhibits more sensitive temperature dependence than the peak at 1.4 THz (F_0), which experiences almost no redshift with increasing temperature (as such, this indicates that the F_0 mode is not correlated to the vacancies).

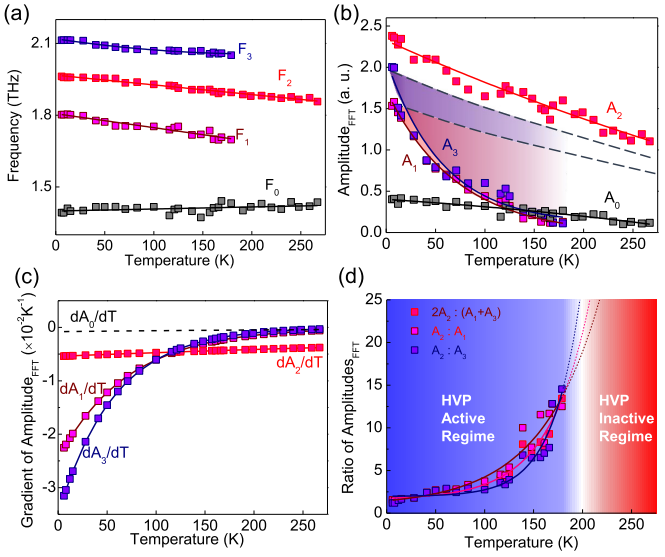

FIG. 3. Temperature dependences of the (a) frequency and (b) amplitude of the CPB, obtained from FFT results in Fig. 2(b). (b) The A_1 and A_3 phonon modes damp faster than the A_2 phonon mode with increasing temperature. Also observed is another coherent optical phonon mode, labeled A_0. (c) Gradient of FFT amplitudes. (d) Ratio between the phonon amplitudes. There is a trend of divergence at about 200 K, dividing the whole temperature range into the active and inactive HVP regimes.

To see the dynamics waning of HVP modes clearer, we further plot the gradient of the FFT amplitude (dA/dT) in Fig. 3(c), which is derived from the FFT amplitude results in Fig. 3(b). The "regular" phonon behavior as exemplified by dA_2/dT is close to a straight line. The gradient of the mode A_0 shares the same regular behavior [Fig. 3(c), dashed line]. However, the two HVP modes exhibit different behaviors, fully exhibiting the waning [Fig. 3(c)]. It can be seen that below 200 K, the slopes of dA_1/dT and dA_3/dT are clearly larger than those of A_2 and A_0; above 200 K, the slopes are close to those of A_2 and A_0. This indicates that one can divide the whole temperature range into two regions: the "HVP active regime" and the "HVP inactive regime" [Fig. 3(d)]. In Fig. 3(d), we explicitly show the ratios between the FFT amplitudes, $A_2 : A_1$, $A_2 : A_3$, and $2A_2 : (A_1 + A_3)$. They exhibit divergences at about 200 K, which means that the amplitudes of A_1 and A_3 are negligible compared with A_2. This defines a boundary between the active and inactive HVP regimes. Ultrafast spectroscopy results in Figs. 3(b) and 3(c) exhibit a clear distinction between the two regimes [Fig. 3(d)].

The aforementioned ultrafast dynamics waning is obtained from the analysis of the frequency-domain FFT results

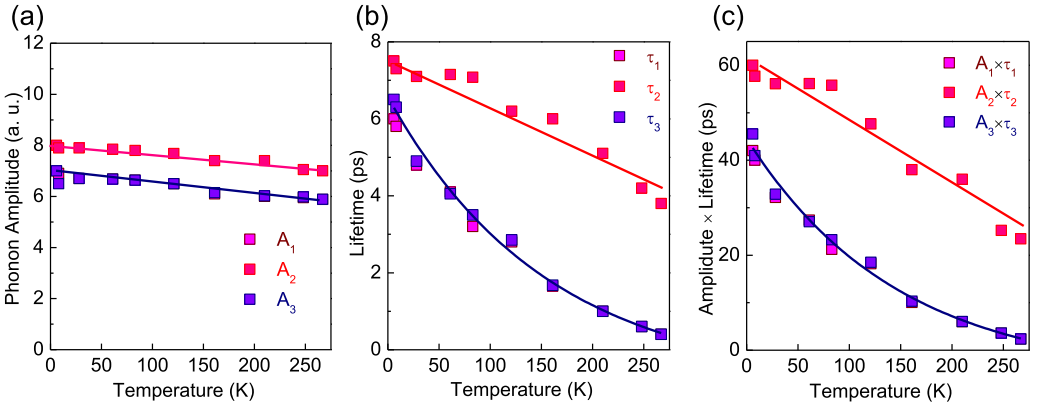

FIG. 4. Temperature dependence of (a) phonon amplitude and (b) lifetime that are obtained from time-domain fitting, without Fourier transformation. (c) The product of the phonon amplitude and lifetime. The dots are time-domain fitting results, while the curves are guides to the eyes.

[Fig. 2(b)]. We simulate the time-domain results directly by summing up three sinusoidal oscillations. For a few typical temperatures, we plot the simulation results (see Supplemental Material [22]) and obtain the phonon amplitudes and lifetimes without directly extracting them from the Fourier transformation. The results are shown in Figs. 4(a) and 4(b). The amplitudes of the three beating phonons do not show dramatic change with increasing temperature [Fig. 4(a)]. Only slight reductions in amplitude are observed and there is no difference between the HVP modes and the central mode. However, the lifetimes of the central phonon and the two HVP modes show a different variation tendency [Fig. 4(b)], which is similar to the results obtained from the FFT amplitudes [Fig. 3(b)]. In order to understand this, we analyze the FFT amplitudes in detail (see Supplemental Material [22]), where we find that the amplitudes of the FFT frequency peak are proportional to the product of the phonon amplitude and the lifetime. Explicitly, we show $A \times \tau$ as a function of temperature [Fig. 4(c)], which is consistent with the FFT amplitude results. The slight difference between the FFT amplitude and the values of $A \times \tau$ can be explained by the fact that there are three beating components in the time-domain oscillation and the FFT amplitude is contributed by three parts together rather than a single component. Nonetheless, the consistency between FFT amplitudes [Fig. 3(b)] and $A \times \tau$ [Fig. 4(c)] supports our analysis. Therefore, the ultrafast dynamics waning we observe in Figs. 3(b) and 3(d) essentially originates from the waning in phonon lifetime of the HVP modes.

In previous investigations of the crystal structure of Cd_3As_2, there has been a discrepancy on whether it is centrosymmetric or noncentrosymmetric [7,8,29], which is attributed to the difficulties in analyzing the subtle difference between the two structures in the x-ray diffraction results. Here, by observing the coherent phonon beating in the ultrafast spectroscopy, especially the dynamics waning of the HVP modes with increasing temperature, we attribute the conflict mainly to the different experimental temperatures used in the experiments (room temperature [8], 100 K [7], and liquid helium temperature [29]).

With temperature increasing from liquid helium temperature to room temperature, the vacancy structure, which is on the two diagonal positions of the As-Cd cube and forms the counter helixes (see Supplemental Material [22]), experiences a progressive change. In each composing block (i.e., the As-Cd cube, see Fig. 5), the As-Cd bond length does not change with temperature because the frequency does not show a difference or merging of frequencies. That means the As atom positions do not change either. However, we observe a lifetime waning in the experiment, which corresponds to the broadening of the vibrations. This reveals that the fluctuation of the As atom position is enhanced with increasing temperature [Figs. 5(a) and 5(b)]. Significantly, at a high temperature above 200 K, in the HVP inactive regime [Fig. 3(d)], only the central phonon peak remains in both time and frequency domains, as shown by our ultrafast results. Thus, one cannot distinguish this vibration mode from that of a structure without vacancies. Below 200 K, the lattice structure is asymmetric. In contrast, from the lattice vibration point of view, the structure becomes indistinguishable from that of a symmetric structure above 200 K. Since the evidence of structural phase transitions at around 200 K or slightly above (this may proceed even to room temperature, as reflected by results in Ref. [27]) is not explicitly presented in the available reports [8], whether there is a structural phase transition at 200 K (or slightly above) is not clear so far. Even though the counter helixes structure might still be there, the electronic band structure of Cd_3As_2, including the Dirac-type topological properties, may not be preserved at higher temperatures. The crossing between the

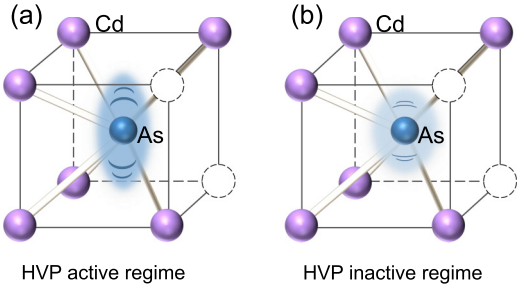

FIG. 5. Schematic diagram of the A_{1g} mode (out-of-plane vibration along the z axis) observed by ultrafast spectrum in the (a) HVP active regime and (b) HVP inactive regime. The smog mimics the real-space position fluctuation, which reflects the phonon broadening.

valence and conduction bands, as well as the degeneracy of the Dirac points, might need reconsideration, taking into account the impact of temperature. This also applies to other similar topological materials. One needs to consider the effect of temperature on the lattice structure, which ultimately possibly modifies the electronic properties.

In conclusion, we carried out an ultrafast optical spectroscopy investigation of the 3D Dirac semimetal Cd_3As_2. We have observed a coherent phonon beating in the crystal, which originates from the HVP modes caused by corkscrew Cd vacancies of opposite chirality. Significantly, such HVP modes show ultrafast dynamics waning, which is immune to the major phonon mode. Our ultrafast dynamics investigation in the lattice degree of freedom thus clearly indicates the crucial role of temperature in investigating the properties of topological materials.

This work was supported by the National Key Research and Development Program of China (Grants No. 2016YFA0300300 and No. 2016YFA0401000), the National Basic Research Program of China (Grant No. 2015CB921301), the National Natural Science Foundation of China (Grants No. 11574383, No. 11274372, No. 11274362, No. 11474330, and No. 11674371), the CAS Interdisciplinary Innovation Team, and the External Cooperation Program of Chinese Academy of Sciences (Grant No. GJHZ1403).

[1] Z. J. Wang, H. M. Weng, Q. S. Wu, X. Dai, and Z. Fang, Three-dimensional Dirac semimetal and quantum transport in Cd_3As_2, Phys. Rev. B **88**, 125427 (2013).

[2] S. M. Young, S. Zaheer, J. C. Y. Teo, C. L. Kane, E. J. Mele, and A. M. Rappe, Dirac Semimetal in Three Dimensions, Phys. Rev. Lett. **108**, 140405 (2012).

[3] Z. K. Liu, J. Jiang, B. Zhou, Z. J. Wang, Y. Zhang, H. M. Weng, D. Prabhakaran, S-K. Mo, H. Peng, P. Dudin, T. Kim, M. Hoesch, Z. Fang, X. Dai, Z. X. Shen, D. L. Fang, Z. Hussain, and Y. L. Chen, A stable three-dimensional topological Dirac semimetal Cd_3As_2, Nat. Mater. **13**, 677 (2014).

[4] S. Borisenko, Q. Gibson, D. Evtushinsky, V. Zabolotnyy, B. Buchner, and R. J. Cava, Experimental Realization of a Three-Dimensional Dirac Semimetal, Phys. Rev. Lett. **113**, 027603 (2014).

[5] H. M. Yi, Z. J. Wang, C. Y. Chen, Y. G. Shi, Y. Feng, A. J. Liang, Z. J. Xie, S. L. He, J. F. He, Y. Y. Peng, X. Liu, Y. Liu, L. Zhao, G. D. Liu, X. L. Dong, J. Zhang, M. Nakatake, M. Arita, K. Shimada, H. Namatame, M. Taniguchi, Z. Y. Xu, C. T. Chen, X. Dai, Z. Fang, and X. J. Zhou, Evidence of topological surface state in three-dimensional Dirac semimetal Cd_3As_2, Sci. Rep. **4**, 6106 (2014).

[6] B. Q. Lv, H. M. Weng, B. B. Fu, X. P. Wang, H. Miao, J. Ma, P. Richard, X. C. Huang, L. X. Zhao, G. F. Chen, Z. Fang, X. Dai, T. Qian, and H. Ding, Experimental Discovery of Weyl Semimetal TaAs, Phys. Rev. X **5**, 031013 (2015).

[7] M. N. Ali, Q. Gibson, S. Jeon, B. B. Zhou, A. Yazdani, and R. J. Cava, The crystal and electronic structures of Cd_3As_2, the three-dimensional electronic analogue to graphene, Inorg. Chem. **53**, 4062 (2014).

[8] G. A. Steigmann and J. Goodyear, The crystal structure of Cd_3As_2, Acta Cryst. B **24**, 1062 (1968).

[9] Y. C. Tian, W. H. Zhang, F. S. Li, Y. L. Wu, Q. Wu, F. Sun, G. Y. Zhou, L. Wang, X. Ma, Q. K. Xue, and J. Zhao, Ultrafast Dynamics Evidence of High Temperature Superconductivity in Single Unit Cell FeSe on $SrTiO_3$, Phys. Rev. Lett. **116**, 107001 (2016).

[10] Jimin Zhao, A. V. Bragas, R. Merlin, and D. J. Lockwood, Magnon squeezing in antiferromagnetic MnF_2 and FeF_2, Phys. Rev. B **73**, 184434 (2006).

[11] N. Cao, Y. F. Wei, Jimin Zhao, S. P. Zhao, Q. S. Yang, Z. G. Zhang, and P. M. Fu, Femtosecond optical detection of quasiparticle dynamics in single-crystal $Bi_2Sr_2CaCu_2O_{8+\delta}$, Chin. Phys. Lett. **25**, 2257 (2008).

[12] D. H. Torchinsky, G. F. Chen, J. L. Luo, N. L. Wang, and N. Gedik, Band-Dependent Quasiparticle Dynamics in Single Crystals of the $Ba_{0.6}K_{0.4}Fe_2As_2$ Superconductor Revealed by Pump-Probe Spectroscopy, Phys. Rev. Lett. **105**, 027005 (2010).

[13] N. Gedik, P. Blake, R. C. Spitzer, J. Orenstein, R. Liang, D. A. Bonn, and W. N. Hardy, Single-quasiparticle stability and quasiparticle-pair decay in $YBa_2Cu_3O_{6.5}$, Phys. Rev. B **70**, 014504 (2004).

[14] J. W. McIver, D. Hsieh, H. Steinberg, P. J. Herrero and N. Gedik, Control over topological insulator photocurrents with light polarization, Nat. Nanotechnol. **7**, 96, (2012).

[15] D. Hsieh, F. Mahmood, J. W. McIver, D. R. Gardner, Y. S. Lee, and N. Gedik, Selective Probing of Photoinduced Charge and Spin Dynamics in the Bulk and Surface of a Topological Insulator, Phys. Rev. Lett. **107**, 077401 (2011).

[16] J. Orenstein and J. E. Moore, Berry phase mechanism for optical gyrotropy in stripe-ordered cuprates, Phys. Rev. B **87**, 165110 (2013).

[17] J. J. Li, J. Chen, D. A. Reis, S. Fahy, and R. Merlin, Optical Probing of Ultrafast Electronic Decay in Bi and Sb with Slow Phonons, Phys. Rev. Lett. **110**, 047401 (2013).

[18] C. Aku-Leh, Jimin Zhao, R. Merlin, J. Menéndez, and M. Cardona, Long-lived optical phonons in ZnO studied with impulsive stimulated Raman scattering, Phys. Rev. B **71**, 205211 (2005).

[19] A. V. Bragas, C. Aku-Leh, S. Costantino, Alka Ingale, J. Zhao, and R. Merlin, Ultrafast optical generation of coherent phonons in $CdTe_{1-x}Se_x$ quantum dots, Phys. Rev. B **69**, 205306 (2004).

[20] S. F. Ge, X. F. Liu, X. F. Qiao, Q. S. Wang, Z. Xu, J. Qiu, P. H. Tan, J. M. Zhao, and D. Sun, Coherent longitudinal acoustic phonon approaching THz frequency in multilayer molybdenum disulphide, Sci. Rep. **4**, 5722 (2014).

[21] Alexander Q. Wu and Xianfan Xu, Ultrafast dynamics of photoexcited coherent phonon in Bi_2Te_3 thin films, Appl. Phys. Lett. **92**, 011108 (2008).

[22] See Supplemental Material at http://link.aps.org/supplemental/10.1103/PhysRevB.95.235108 for additional experimental data and their analyses.

[23] J. Y. Feng, Y. Pang, D. S. Wu, Z. J. Wang, H. M. Weng, J. Q. Li, X. Dai, Z. Fang, Y. G. Shi, and L. Lu, Large linear

magnetoresistance in Dirac semimetal Cd_3As_2 with Fermi surfaces close to the Dirac points, Phys. Rev. B **92**, 081306(R) (2015).

[24] J. M. Zhao, A. V. Bragas, D. J. Lockwood, and R. Merlin, Magnon Squeezing in an Antiferromagnet: Reducing the Spin Noise below the Standard Quantum Limit, Phys. Rev. Lett. **93**, 107203 (2004).

[25] R. Merlin, Generating coherent THz phonons with light pulses, Solid State Commun. **102**, 207 (1997).

[26] D. M. Riffe and A. J. Sabbah, Coherent excitation of the optic phonon in Si: Transiently stimulated Raman scattering with a finite-lifetime electronic excitation, Phys. Rev. B **76**, 085207 (2007).

[27] S. Jandl, S. Desgreniers, C. Carlone and M. J. Aubin, The Raman spectrum of Cd_3As_2, J. Raman Spectrosc. **15**, 137 (1984).

[28] J. Weszka, M. Renucci, and A. Zwick, Some aspects of Raman scattering in Cd_3As_2 single crystals, Phys. Stat. Sol. (b) **133**, 57 (1986).

[29] R. Sankar, M. Neupane, S. Y. Xu, C. J. Butler, I. Zeljkovic, I. Panneer Muthuselvam, F.-T. Huang, S. T. Guo, Sunil K. Karna, M. W. Chu, W. L. Lee, M. T. Lin, R. Jayavel, V. Madhavan, M. Z. Hasan and F. C. Chou, Large single crystal growth, transport property, and spectroscopic characterizations of three-dimensional Dirac semimetal Cd_3As_2, Sci. Rep. **5**, 12966 (2015).